

Lidar Observations of Stratospheric- Mesospheric Density Structure and Its' Climatology at Logan Utah

Robert D. Sears*, V. B. Wickwar^{##}

(*RDS, Research & Development Sciences, LLC, Albuquerque NM 87111),

([#]VBW, Utah State University, Logan UT, 84322)

ABSTRACT

Data obtained from the USU incoherent backscatter lidar at Logan Utah during the interval 1994 through 1998 has been analyzed in terms of the climatology of stratospheric and lower mesospheric mean density and density variance $(\delta\rho/\rho)^2$ vs. altitude. The total database consists of over 322 nights of cloud-free data over the altitude range, 40 to 90 km. We selected a subset of 142 days (886 hours) of the highest signal to noise ratio data for the analysis. The temporal and spatial resolutions were 2 minutes and 112.5 meters respectively. We compared the mean density profiles, normalized to MSISe90 on a monthly and seasonal basis to MSISe90. The mean density profiles compared well with the MSISe90 model with the following exceptions. The measured densities were less than MSISe90 predictions in the 45 to 80 km range by up to 10% in the 1st calendar quarter, and greater than MSISe90 density predictions in the last calendar quarter, by about 8 to 10 %, but over a narrower altitude range. The density variance profiles $(\delta\rho/\rho)^2$ are proportional to the mean free energy of the atmospheric gravity wave and turbulent structure. The density variance altitude profiles generally had two components: a low altitude component that appeared to have an average variance vs. altitude slope below the saturation value, proportional to twice the scale height. An upper altitude component had a variance slope greater than the saturation value thus suggesting a region of unstable wave propagation. The magnitude and slope of the density variance profiles varied greatly from day to day within a month, and the monthly averages varied considerably both in magnitude and behavior of the transition region between the two regimes. In terms of free energy in the lower altitude range, below about 70 km, the estimated free energy varied from about 6 to 10 J/kg to as much as 57 J/kg in April and ~ 40 J/kg in January and October. The daily variability in free energy at 50 km within a given month was in the range of a factor of 5 to 10, therefore some months having fewer daily data sets may be skewed statistically. Some seasonal dependence may be inferred after eliminating months that had a statistically deficient number of nightly samples. The observed range of free energy was consistent with that derived from Lidar observations at other sites.

Keywords: Rayleigh LIDAR, atmospheric structure, Atmospheric density profiles, atmospheric free energy profiles. Atmospheric turbulence and gravity waves.

1. INTRODUCTION

Rayleigh LIDAR systems at a number of worldwide sites (Western Ontario, Haute Provence, Greenland, etc.) have been utilized to measure atmospheric density and temperature profiles. A desired goal of these experiments is validate atmospheric models such as MSIS and to identify and quantify the detailed atmospheric hydrodynamic processes that control the observed temperature and density profiles. These atmospheric processes and their effects upon the atmospheric chemiluminescence create, for example, the OH-layer structure observed near the mesopause region at about 90 km. Establishing an empirical climatology for density and temperature profiles and free energy $(\sim (\delta\rho/\rho)^2, (\delta T/T)^2)$ at a variety of sites is an important element in worldwide modeling of energy transport through the stratosphere and mesosphere. The atmospheric density and density variance climatology data from Logan Utah presented in this paper are a contributory element to the overall worldwide energy transport modeling effort.

* rdsears@highfiber.com, tel/fax 505-296-5609, Research & Development Sciences, LLC., 5021 Calle Del Cielo, Albuquerque NM 87111-2913.

[#] wickwar@aeronomy.cass.usu.edu, tel 435-797-3641, Utah State University, Center for Atmospheric & Space Sciences (CASS), Logan UT

One of the major contributors to stratospheric- mesospheric energy balance is the propagation of gravity waves from the troposphere. These gravity waves, caused by convective disturbances, orographic effects, jet stream instabilities or other physical causes, contribute hydrodynamic free energy throughout the stratosphere and mesosphere. The AG waves generated at lower altitudes will be filtered out in critical layers determined by temperature profile and/or wind shear, or will grow in amplitude with altitude (e-folding amplitude distance $\sim 2H$) until energy saturation or wave-breaking conditions are encountered.

The daily, seasonal, and annual profiles of mean density relate to the overall climatology of the atmosphere, can be used to validate predictive models of atmospheric density and temperature behavior vs. altitude. , Atmospheric density perturbations $(\delta\rho/\rho)^2$ are a measure of the free energy in the atmosphere contained in turbulence and gravity wave perturbations.

The temperature morphology and climatology of the stratosphere and mesosphere have been investigated by a number of groups, at a variety of worldwide sites by Hauchecorne et al (1991)¹, Sica et. al. (1995)², and Wickwar et al (2001)^{3,4}. The Logan Utah site is distinguished from the other mid-latitude sites in at least one important factors: the site is in a mountainous region expected to generate a high level of orographic gravity waves during appropriate seasonal wind conditions.

We analyzed data from the USU Rayleigh LIDAR to determine climatology of the mean density profiles, $\rho(\text{alt})$ and normalized mean density variance profiles, $(\delta\rho/\rho)^2$ vs. altitude on a daily, monthly, and seasonal basis. We compared measurements of $\rho(\text{alt})$ to standard models for atmospheric density profile such as MSISe90 (Hedin, 1991)⁵. We also computed the climatology of the normalized mean density variance profiles, $(\delta\rho/\rho)^2$ in order to associate the stratosphere and mesosphere free energy levels with the presence of gravity waves. We also investigated the power spectral density of the density fluctuations to attempt to determine the change in PSD caused by coherent wavelike effects as opposed to nominal quiet conditions.

2. THE USU LIDAR EXPERIMENT

2.1 LIDAR Description

The Utah State University (USU) Lidar is located in the Cache Valley on the USU campus. Wickwar et. al. (1997, 2001)³ described the Lidar in detail and described work accomplished to date relating to derivation of temperature profiles from the Raleigh backscattered signal. Table 1 summarizes the relevant features of the lidar and specifically identifies the high altitude temporal resolutions built into the data acquisition system. The altitude resolution value was chosen to enable analysis if the atmospheric dynamical processes on a scale much smaller than the vertical scale height or the anticipated vertical wavelengths of propagating gravity waves. Similarly, the temporal resolution was chosen to be smaller than the Brunt-Vaisala (atmospheric buoyancy) period over the altitude range of interest, nominally 40 to ~ 90 km.

Table 1 Logan UT LIDAR Characteristics

Site Coordinates	41.7N, 111.8W, 1.500 km altitude
Wavelength	532 nm (Doubled NdYag)
Energy/pulse	800 mJ, 600 mJ*
PRF	30 Hz
Power Aperture Product	3.42 w-m², 2.57 w-m²
Altitude Range	40 - 90 km
Altitude Resolution	37.5 meters (binned to 112.5 m)
Temporal Resolution	2 minutes (3600 pulses)
* Two different lasers were used during the course of the measurements	

The Lidar technology provides key elements for our analysis. The high spatial (112.5 m) and high temporal (2 minutes) resolution Rayleigh backscatter signals allow calculation atmospheric density on scale sizes smaller than the vertical wavelength of most gravity waves, and on a temporal scale smaller than the Brunt-Vaisala period (the dividing time between acoustic mode and gravity mode waves). Hence, by selecting post-processing altitude-time bins, the gravity wave energy dissipation and power spectral density can be computed by optimal techniques for reduction of the variance in the desired atmospheric parameters. Sears et al (1995)⁶ described this technique.

2.2 Data Summary

We used a very extensive data sample from the USU Lidar, extending over 322 days from 1994-1998. This data sample was severely edited to eliminate periods of low apparent gain (caused by haze or continuous thin clouds) or those nights that contained intermittent gaps caused by clouds. Table 2 summarizes the data statistics for the analysis: of the input 322 days an edited dataset of 142 days (886 hours) of useful data were applied to the analysis. The total number of days of observations and days selected are a function of local weather, operator availability (exams), and system downtime (a small fraction). Days of full moon were not selected, but as will be reported later, partial moon, and thin cloud nights were included in the analysis as long as the detrending processes were successful.

Table 2 Data Statistics for 1994-1998 Measurement Interval

MONTH	Total Days	Days Used	Hours Used
JANUARY	16	10	78.7
FEBRUARY	33	9	77.3
MARCH	36	12	87.6
APRIL	9	6	27.7
MAY	6	3	11.1
JUNE	23	17	74.6
JULY	22	15	60.1
AUGUST	48	22	132.7
SEPTEMBER	54	23	151.7
OCTOBER	42	14	96.2
NOVEMBER	11	4	31.6
DECEMBER	22	7	56.7
SUM	322	142	886

3. LIDAR DATA ANALYSIS AND RESULTS

3.1 Data Conditioning and Detrending

The LIDAR data sets for each nightly operating period are organized as a 2-D matrix array, IM, dimensioned in altitude and time. Each nightly data array is truncated in altitude and separated into distinct altitude regimes: the experimental range, 40 – 90 km, and the noise correction range above the experiment altitude range, about 95 to 100 km. The format of the data array is an NxM matrix where N = 1247 altitude pixels (invariant over the analysis) and M = T 2-minute time pixels (varying with the data set).

We instituted two detrending processes for the LIDAR data: temporal detrending of the background noise vs. time over the nightly data interval and temporal detrending of the overall signal levels in the data range. The noise detrending accounts for temporal trends in background count rates caused by changes in the astronomical backgrounds including scattered moonlight and starlight, backscattered ground illumination from haze and clouds, and any possible light leaks into the experimental apparatus. The temporal detrending process also accommodates changes of LIDAR system gain over the nightly intervals (not definitively observed) and possible changes in atmospheric transmission (at lower altitudes) caused by thin clouds, haze, etc (definitely observed).

Noise Detrending

We formulated a temporal vector to represent the mean background noise vs. time for each nightly data set by integrating the background count rate (counts/altitude bin) over the altitude interval in the noise window. The temporal background noise vector was subtracted from the time-altitude matrix representing the data set. This noise subtraction process is similar to that used by several other LIDAR groups.

Temporal Detrending

We corrected the data samples for temporal variations caused by atmospheric transmission variability (e.g. by thin clouds) and system gain variability (either laser output or photon detection efficiency changes) over each nightly observation interval. We computed a temporal vector, VT, containing the total return signal (counts/ altitude bin) per time interval over

the experiment altitude range and normalized it by its temporal average VT. A normalization vector then is constructed to multiply by the data matrix to bring the entire data sample to the same total return in data matrix DNNM.

$$VT_t = \sum_{z_l}^{z_u} DM_{z,t} \quad VTN_t = VT_t / \overline{VT} \quad \overline{VT} = (T^{-1}) \sum_t VT_t \quad DNNM_{z,t} = VTN_t * DM_{z,t}$$

As described above, we normalized the temporal variations of the data sample by multiplying the experimental data matrix by the ratio of the temporal vector VT to its average, \overline{VT} over the nightly data interval.

Figure 1 illustrates the results of this temporal detrending when thin clouds are present. The process does not work well when thick clouds are present for a significant interval. After application of this technique to hundreds of data samples, we have found many cases, where we can correct for thin cloud transmission effects: we have not found any cases where temporal variability of system lidar power or detection efficiency effects was significant.

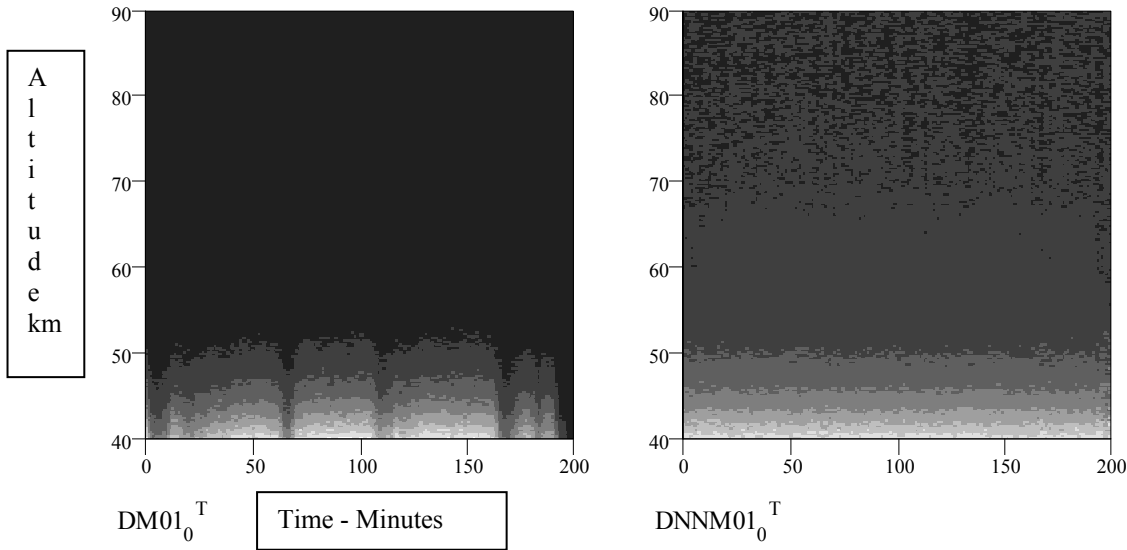


Figure 1 Temporal detrending results. Left panel shows altitude-time plot before detrending is applied. Right Panel shows equivalent plot after temporal detrending.

3.2 Mean Density Computation – Normalization to MSIS90

We computed the nightly mean count rate profiles from the detrended data matrix DNNM by taking the temporal averages over each DNNM altitude bin. The mean density profiles are produced by normalizing the count rate profiles to the atmospheric mean density at 40 km, as computed for the Logan Utah site using MSIS90e. We used the midnight, mid-month density profiles as being the most representative of the nightly data samples and their monthly averages. In order to compare the count rate vs. altitude with density profiles, it is necessary to normalize the count rate for the range effect. For an incoherent radar having a fully illuminated receiving telescope FOV, it is well known that the photon counts/altitude bin fall off as range², therefore all of the count profile data were normalized to the 40 km value by the ratio: $R = (\text{bin altitude} - \text{km}/40)^2$.

The plots presented in Figures 2 to 5 are a result of a variable passband adaptive filter, which has an effective vertical passband of about one scale height, $H \sim 7$ km. This filter obscures some of the wavelike features found in the analysis results using a smaller aperture filter.

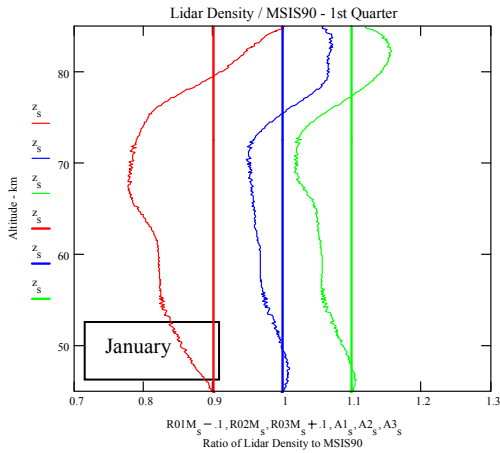


Figure 2 Ratio of LIDAR Data to MSIS90e. First quarter results. Monthly curves are Separated by ± 0.1 on the horizontal axis.

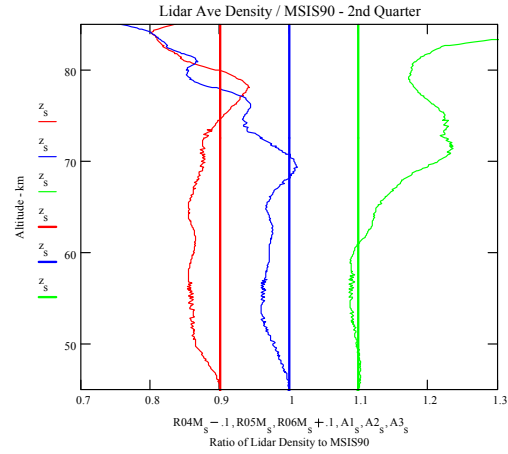


Figure 3 Ratio of LIDAR Data to MSIS90e. Second Quarter. Plot as in Figure 2

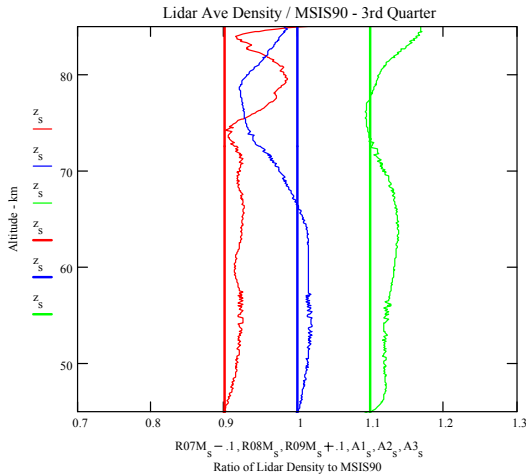


Figure 4 Ratio of LIDAR Data to MSIS90e. Third quarter. Plot as in Figure 2.

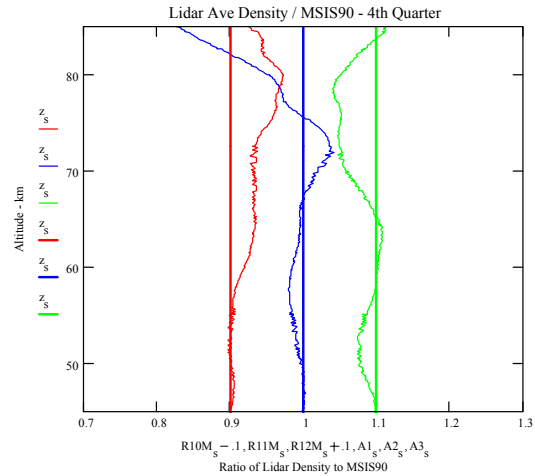


Figure 5 Ratio of LIDAR Data to MSIS90e. Fourth Quarter. Plot as in Figure 2.

3.3 Density Profiles Climatology and Comparison to MSIS90

After normalization of the range-corrected photon count profiles to the MSIS90 values at 40 km, we compared the monthly mean density profiles to MSIS90 by ratioing the LIDAR experiment values to the MSIS90 model values. Summarizing these results presented in Figures 2 through 5, we can make the following conclusions relating to the monthly and seasonal comparison of experiment and model:

- WINTER QUARTER (Figure 2 plus April in Figure 2)
 - Lidar data underlies predicted MSIS90 density in the 45 to ~75 km altitude range.
 - The maximum difference is ~ 10% at 70 km.
 - Lidar density profiles are larger than MSIS90 above ~ 75 km by < 10 percent.
- SPRING QUARTER (Figure 3)
 - Lidar density is significantly lower than MSIS90 above 70 km in May and strongly above MSIS90 in June over the same altitude range.
 - Lidar density is ~ 5 % below MSIS90 between 50 and 70 km in April and May .

- SUMMER QUARTER (Figure 4)
 - Lidar density difference $\sim +5\%$ compared to MSISe90 in the 45-70 km range
- FALL QUARTER (Figure 5)
 - Lidar density is greater than MSISe90 by about 8% in October in the 60- 80 km range.
 - November Lidar density has a large negative excursion above 75 km.
 - Lidar density data in December is up to 5% less than MSISe90 between 65 and 85 km.

We also note that the number of days included in each comparison varies from 3 and 4 days respectively for May and November vs. 22 and 23 days respectively for August and September. We have no reason to believe that the selection process influenced the monthly average density profiles and their relationship to MSISe90, but the statistical selection process must always be a concern when processing geophysical data.

3.4 Density Variance Computation

We computed the density variances following the technique published by Thayer et al(1997)⁷ with several significant differences. We followed the standard procedure of subtracting the Poisson photon counting variance profile (equal to the mean count rate vs. altitude) from the total count rate variance (per altitude bin), then applying an adaptive filter to reduce statistical variance vs. altitude after the daily $(dr/r)^2$ calculation. The analysis in this paper has a major difference from the standard procedure in that the variances are computed in the time domain rather than the spatial (altitude) domain after noise and temporal detrending of each nightly dataset. The density variance is directly proportional to the excess count rate variance in that all of the range corrections and density normalization factors are removed by the normalization.

Figure 6 presents an example of the results of this analysis process for one month, January, that has a significant number of daily data samples. This figure shows 10 nightly averages of, the average value for the month and a line depicting the conservative energy growth rate for an atmosphere with a 7.4 km scale height. The conservative energy growth rate curve is normalized to the value used by Whitway and Carswell (1995). Table 3 summarizes the monthly average behavior statistics for the data analyzed.

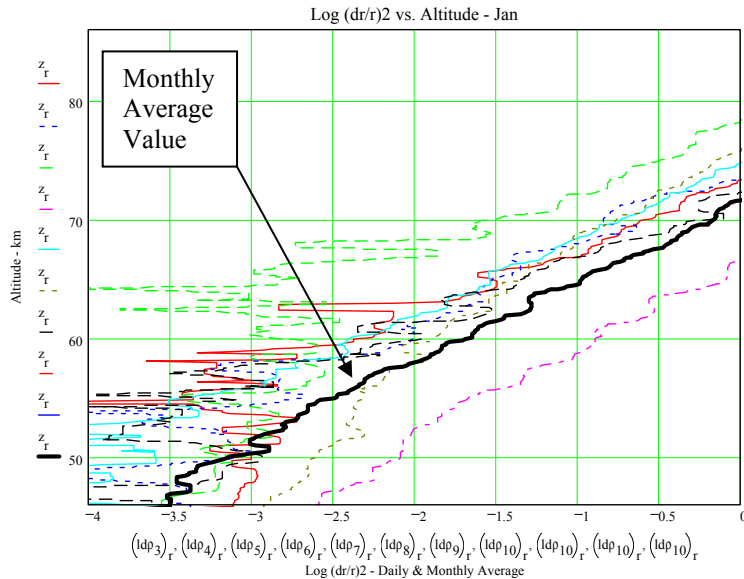


Figure 6 Daily Density Variance $(dr/r)^2$ vs. Altitude Profiles and Monthly Average for January

The January $(dr/r)^2$ profiles exhibit characteristics common to every month, except for months having so few data samples that we cannot be sure of their statistical validity. Each month shows a number of days that have "conservative" behavior at lower altitudes, defined as the average slope of $(dr/r)^2$ vs altitude is less than that of the "conservative" line. Above some critical altitude, usually exhibited as a cusp in the daily (and often the monthly average) curves, the slope of $(\delta\rho/\rho)^2$ vs

altitude increases – this is exhibited by a flatter slope in the figures because the altitude- $(\delta\rho/\rho)^2$ axes are reversed. Very few of the days analyzed exhibit a "non-conservative" slope over the entire altitude range, and a few days exhibit anomalous behavior.

The atmospheric free energy is related to the normalized density variance by the formula $E = 0.5 (g/N)^2 (\delta\rho/\rho)^2$. Because the Brunt-Vaisala period $N \sim 300$ sec is a slowly varying function with altitude except under conditions of extreme temperature gradients, one may obtain a heuristic view of the free energy changes in the atmosphere over the altitude range of the measurements, 40 – 90 km. For example, a 1 percent change in $(\delta\rho/\rho)^2$ corresponds approximately to free energy $E \sim 10$ Joule/kg at 50 km. Therefore an examination of the altitude profiles of $(\delta\rho/\rho)^2$ on a daily and monthly averaged basis may yield some insight into the physics of the energy propagation and dissipation processes. Strong variations in the value of $(\delta\rho/\rho)^2$ and implicitly, the free energy, also yields some information on the temperature gradient structure over the density measurement range.

Based upon study of the daily and monthly plots of $(dr/r)^2$ we sought to identify parameters that might lend more insight regarding the climatological behavior of the free energy profiles. These parameters are simplified as follows: the low altitude value of density variance – nominally at 50 km- in the conservative energy growth range and the transition altitude between the conservative growth region (low altitude) and the higher altitude "non-conservative region.

3.5 Climatology of Density Variance vs. Altitude

We computed the monthly average density variance values, $(\delta\rho/\rho)^2$ vs altitude. These values are plotted in Figures 7 through 10. Several behavior patterns may be deduced from these plots. Two altitude regimes are identifiable: at low altitudes the normalized density variance profiles are characterized by a wavelike or cusp-like behavior over which the average $(\delta\rho/\rho)^2$ slope behaves more or less conservatively, ie. the e-folding growth of $(\delta\rho/\rho)^2$ is less than the conservative energy growth rate that is proportional to the density scale height, ~ 7 km. A transition altitude is observed above which the growth of $(\delta\rho/\rho)^2$ vs altitude is greater than the conservative growth rate, thus posing a problem of energy conservation. The slope of the "non-conservative

Table 3 Statistics of Density Variance $(\delta\rho/\rho)^2$ Altitude Profiles

Month	Days	Low Altitude Conservative	Transition Altitude - km	Conservative All Altitudes	Super-Conservative All Altitudes
Jan	10	6	50-60 (55)*	0	2
Feb	9	7	50-65 (57)	0	2
Mar	10	5	50-70 (60)	1	4
April	6	4	65-80 (72)	0	2
May	3	3	49-77 (63)	0	0
June	14	11	50-81 (65)	2#(almost)	2# (almost)
July	14	11	58-82 (70)	0	3
August	14	12	66-80 (73)	1#	1#
Sept	14	13	58-76 (72)	1	0
Oct	14	13	67-83 (75)	0	1
Nov	4	4	50-60 (55)	0	0
Dec	7	6	48-60 (54)	0	0

* (xx) indicated median altitude
indicates that curve may be placed in either category

The low altitude free energy (normalized at 50 km) may be compared with data obtained by other investigators if we assume some nominal value for the Brunt-Vaisala Frequency (period ~ 300 sec, $N \sim 2\pi/300$). Table 4 summarizes this comparison from a selection of the literature on Lidar density variations. The numerical values are compared on a monthly basis.

Table 4 Comparison of Free Energy Inferred from Logan Lidar Data with Other Locations

Month	Jan	Feb	Mar	Apr	May	Jun	Jul	Aug	Sep	Oct	Nov	Dec
Location												
Logan	40	10	6	57	30	<1	148*/30	27	<10	36	<3	6
Toronto⁸	30	-	17	-	-	19	-	-	10	-	-	-
Aberystwyth⁹	-	16-100	-	-	-	5-10						
*Identifies anomalous values that are more accurately represented by the medians.												

Table 4 does not clearly indicate any significant difference in climatology between the sites, but this comparison is limited by the lack of statistical coverage and an approximate value for the Brunt-Vaisala frequency in the Logan data. A more clear-cut and meaningful comparison can be made when the local gravity wave generation and propagation conditions, such as meteorological and orographic sources, are better defined. A more complete comparison of free energy conditions vs. altitude will be made when the temperature profiles from Logan are included in the analysis, and when a more complete climatology is available from the locations cited above as well as other Lidar sites.

4. DISCUSSION OF RESULTS

4.1 Density Climatology

The LIDAR density observations at Logan UT show significant departures in the 5 to 10 percent range from the MSIS390 model in all calendar quarters depending on altitude interval. Whether the differences, outlined in Table 3 are correlated with global tidal or gravity wave modes, or local orographic wave generation is undetermined at present. We do not see any clearly defined seasonal behavior in either low-altitude (~40-70 km,) or high-altitude (> 70 km) components. The data appears to show that the LIDAR density measurements are consistently lower than MSISe90 in the winter and spring at lower altitudes and slightly above MSISe90 predictions the rest of the year. High altitude density behavior appears more chaotic at least as compared with MSISe90.

4.2 Density Variance Results and Climatology

Density variance results and free energy estimates show significant variations, up to a factor of 5 or so, when comparing the daily averages with the monthly averages. Because the daily variability of $(\delta\rho/\rho)^2$ vary so much, and often have anomalously high values, the monthly averages appeared to be skewed upon occasion by anomalously high values. In these cases, the monthly median values, or averages computed after eliminating apparent anomalies may be a more physically correct $(\delta\rho/\rho)^2$ representation of at least the lower altitude $(\delta\rho/\rho)^2$ results and the free energy implied from these values.

In the lower altitude range, below the transition altitude, the density variance and estimated free energy behavior appears to agree with the values found by some other observers. We did not try at this stage to find all of the density variance climatology results. We found some evidence for periodic variability in density structure below the transition altitude. This variability may be similar to that found by other observers in the density variance profiles and in temperature profiles. Figure 7 shows this effect most clearly in a monthly averaged profile. Daily profiles also show this behavior. Existence of this phenomenology is consistent with other observations of wavelike structure that exist in the upper stratosphere and lower mesosphere.

In the altitude range, above the transition altitude, a large preponderance of the data presented in this publication shows an increasing value of $(\delta\rho/\rho)^2$ at a rate greater than the conservation curve. Based upon the temperature lapse rates for this region and their day by day variations which sometimes reach super-adiabatic slopes, some degree of non-adiabatic energy transfer might be expected. We did not expect that most of the density variance would show this behavior. A great deal of effort was spent to validate the computations, especially the detrending routines, in the sense of eliminating statistical or analytical artifacts. We found that the de-noising and temporal detrending routines did not produce the observed "super-conservative" behavior for any of the days that already exhibited it at any level of processing.

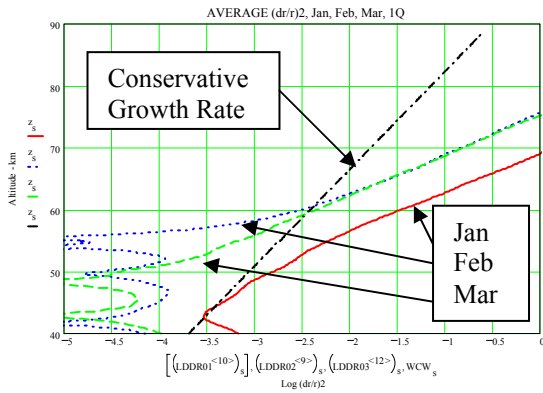


Figure 7 Monthly Average Density Variance Profiles – 1st Quarter

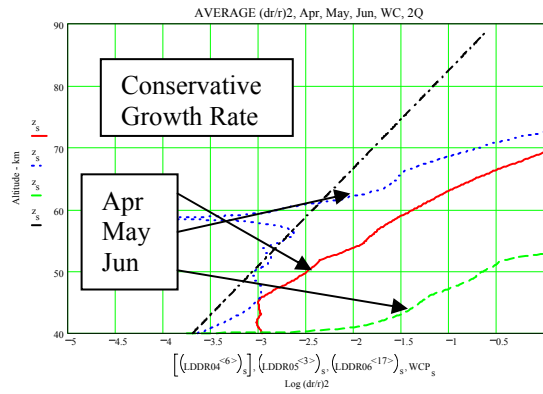


Figure 8 Monthly Average Density Variance Profiles - 2nd Quarter

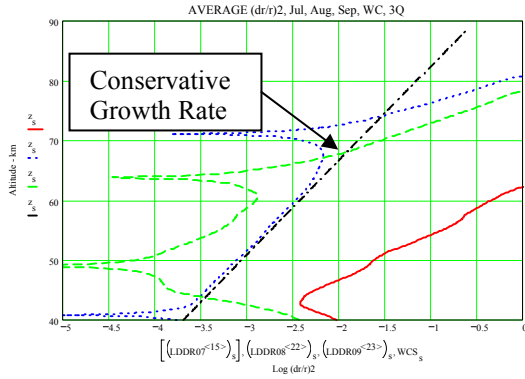


Figure 9 Density Variance Profiles – 3rd Quarter

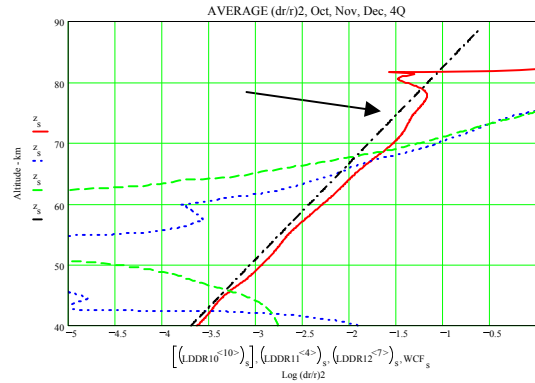


Figure 10 Density Variance Profiles – 4th Quarter

We forward the hypothesis that the transition altitude and "super-conservative" behavior is a consequence of the true three-dimensional nature of the gravity wave field. We are measuring the variance profile using temporal data only. Other observers have measured the variance profile using altitude-dependent variances only. Following the suggestion of Gardner et al (1998)¹⁰ regarding the inseparability of the gravity wave spectrum, it is proposed that temporal and/or spatial measurements of density variance by themselves do not constitute a complete picture of the total variance of the gravity wave field. Empirical models (Strugala et al, 1993)¹¹ of atmospheric structure especially at mesospheric heights account for the increasing spatial asymmetry of the density and temperature correlation functions. Additionally, the temporal variances reported in this paper would only be increased above the altitude-derived variances because the neutral winds would convect frozen-in horizontal structure through the lidar field, producing a variance component in excess of that observed in the vertical dimension.

We conclude from these data sets and their comparison to density variance data obtained by the conventional altitude computation that at mesopause altitudes, above some transition altitude, measurement of the true atmospheric variance requires both altitude and temporal dimensions. This will be carried out in the future on the data set referenced herein.

5. ACKNOWLEDGEMENTS

The USU LIDAR system is supported by the National Science Foundation under Grant No. ATM-9714789. The Independent Research Program of Research and Development Sciences, LLC supported the analysis of these data.

6. REFERENCES

-
- ¹ A. Hauchecorne, J. -L Chanin, and P. Keckhut, "Climatology and trends of the middle atmosphere temperature (33-87 km) as seen by Rayleigh Lidar over the south of France," *J. Geophys. Res.* **96**, 15297-15301, 1991.
 - ² R. J. Sica, S. Sargoytchev, P. S. Argall, E. F. Borra, L. Girard, C. T. Sparrow, and S Flatt, "Lidar measurements taken with a large aperture liquid mirror – 1. Rayleigh scatter system," *Appl. Optics*, **34**, 6925-6936, (1995).
 - ³ V. B. Wickwar, K. C. Beissner, T. D. Wilkerson, S. C. Collins, J. M. Maloney, J. W. Meriwether, and X. Gaio, "Climatology of mesospheric temperature profiles observed with the Consortium Rayleigh-scatter lidar at Logan Utah," in *Advances in Atmospheric Remote Sensing with Lidar*, ed. A Ansmann, R. Neuber, P. Rairoux and U. Wandinger, pp. 557-560, Springer Verlag, Berlin, 1997.
 - ⁴ V. B. Wickwar, T. D. Wilkerson, M. Hammond, and J. P. Herron, "Mesospheric temperature observations at the USU/CASS Atmospheric Lidar Observatory (ALO)," in *Remote Sensing of the Atmosphere, Environment, and Space*, vol. 4153, pp. 272-284, SPIE, Sendai, Japan, 2001.
 - ⁵ A. E. Hedin, "Extension of the MSIS thermospheric model into the middle and lower atmosphere," *J. Geophys. Res.* **96**, 15297-15309, 1991.
 - ⁶ R. D. Sears, T. D. Wilkerson, V. B. Wickwar, J. M. Maloney, and S. C. Collins, "Multi-dimensional Power Spectral Analysis of Structure in the Stratosphere and Mesosphere Observed by Rayleigh Scatter Lidar," in *Proceedings of International Laser Radar Conference*, Berlin German, July 1996.
 - ⁷ J. P. Thayer, N. B. Nielsen, R. E. Warren, C. J. Heinselman, and J. Sohn, "Rayleigh lidar system for middle atmosphere research in the arctic," *Opt. Eng.* **36**, 2045-2061, July 1997.
 - ⁸ J. A. Whiteway and A. I. Carswell, "Lidar observations of gravity wave activity in the upper stratosphere over Toronto," *J. Geophys Res.* **100**, 14113-14124, July 20, 1995.
 - ⁹ A. J. McDonald, L. Thomas, and D. P. Waring, "Night-to-night changes in the characteristics of gravity waves at stratospheric and lower mesospheric heights," *Ann. Geophysicae*, **16**, 229-237 (1998)
 - ¹⁰ C. S. Gardner, S. J. Franke, W. Yang, X. Tao, and J. R. Yu, "Interpretation of gravity waves observed in the mesopause region at Starfire Optical Range, New Mexico: Strong evidence for nonseparable intrinsic (m,w) spectra," *J. Geophys. Res.* **103**, 8699-8713, 1998.
 - ¹¹ L. A. Strugala, R. D. Sears, J. E. Newt, and B. J. Herman, "Production of statistically non-stationary stochastic structure realizations for IR background scene simulations," *Optical Engineering*, May 1993.